Evaluation of the TierPET system

S. Weber, H. Herzog*, M. Cremer*, R. Engels, K. Hamacher+, F. Kehren*, H. Muehlensiepen*, L. Ploux, R. Reinartz, P. Reinhart, F. Rongen, F. Sonnenberg, H. H. Coenen+ and H. Halling
Zentrallabor fuer Elektronik, *Institut fuer Medizin, +Institut fuer Nuklearchemie
Forschungszentrum Juelich GmbH, D-52425 Juelich

Abstract

The TierPET system, a high resolution 3D positron emission tomograph, has been developed to perform small animal positron emission tomography (PET) studies. High resolution PET opens the possibility to perform animal trials without the need for vivisection. This reduces the number of animals and the costs for such experiments, for example concerning the development of new radiopharmaceuticals. The scanner uses two orthogonal pairs of detectors consisting of arrays of small individual YAP crystals coupled to position sensitive photomultipliers. The center-detector distance may be varied to improve either sensitivity or spatial resolution. The spatial resolution of the scanner is 2.1 mm.

I. INTRODUCTION

The development of new radiopharmaceuticals is vital for the innovative development of nuclear medicine. New radiopharmaceuticals are able to provide essential information concerning physiology or pathophysiology of tissue. Also drug development and evaluation can be improved using a positron-emitting isotopically labelled version of the new drug for studying pharmacokinetics *in vivo*. High resolution positron emission tomography is a means to assess the mechanisms and efficacy of new pharmaceutical agents at a very early stage in their development, thereby increasing the speed and reducing the cost of drug development.

In clinical research it is of major interest to obtain new information concerning human diseases and to measure the effectiveness and action of a therapy, for example pharmacological intervention, radiotherapy or transplantation. As a first stage of research, most experiments have to be performed with animals. Due to the noninvasive character of PET, it is possible to perform repeated scans in the same animal so that the progress of a disease as well as its treatment efficacy and mechanism can be studied.

Possible applications of high resolution PET, especially interesting for the brain research in our research center, are brain receptor binding studies. An important region of interest for receptor studies is the striatum of the rat, which is a paired structure with a separation of about 8 mm. Each part has a diameter of about 2 mm. Other applications may be studies of tumor growth and treatment.

The advantages of high resolution PET for animal trials have led to a growing interest in these instruments. Various scanners have been developed [1]-[7] or are under development [8],[9].

We have built a high resolution PET scanner, the TierPET, based on YAP matrices coupled to position sensitive photomultiplier tubes. The geometry of the scanner is flexible and allows the choice between different center-detector distances.

II. SYSTEM DESCRIPTION

Figure 1 shows a picture of the TierPET. The scanner uses four planar detectors consisting of matrices of small single Yttrium Aluminium Perovskit (YAP) scintillator crystals [10] coupled to position sensitive photomultiplier tubes. Lead frames are used as a clamping fixture for the crystals and serve as an additional shielding against scattered photons.

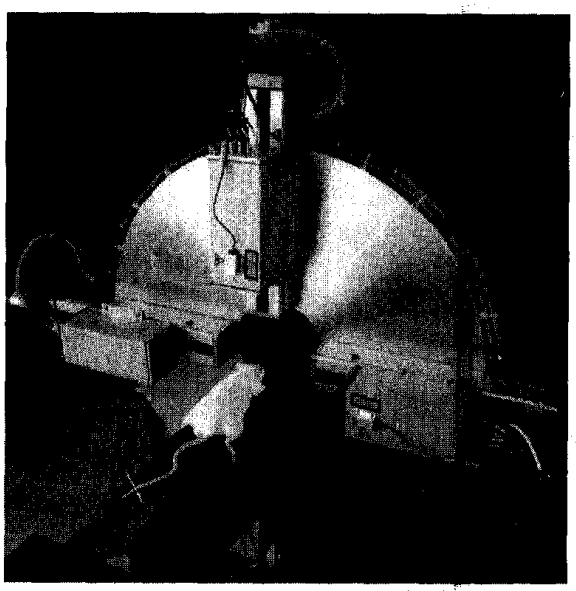

Figure 1: The TierPET

One detector block consists of 20 x 20 small individual scintillator crystals of dimensions 2 x 2 x 15 mm^3 which are optically isolated by thin reflective layers. The 400 single crystals are closely packed and glued together (figure 2). The crystal matrix is coupled to a position sensitive photomultiplier tube with crossed wire anode (Hamamatsu R2487). Such a detector block is able to perform a precise determination of the position.

The crystal dimensions and the detector layout are the result of extensive simulations which respect to sensitivity, spatial resolution and additional parameters like parallax error or scatter effects [11],[12].

The four detector modules are mounted on an aluminium wheel which can be rotated by 90° during a scan by stepper

0018-9499/99$10.00

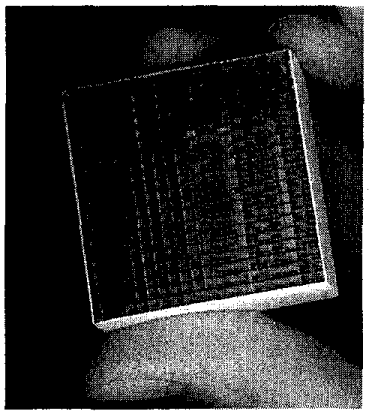

Figure 2: YAP crystal matrix

motors. The center-detector distance can be changed from 8 to 20 cm.

The data acquisition in 3D mode is performed by a PC which also controls the stepper motors. The data are taken in list mode with ADC values for position as well as energy information, and it is possible to include time marks.

The main characteristics of the TierPET are summarized in table 1.

Table 1
Main characteristics of the TierPET

Detector	
No. of detectors	4
Scintillator material	Yttrium Aluminium Perovskit (YAP)
Crystal size	2 x 2 x 15 mm^3
Number of crystals	20 x 20 crystals per module
Crystal pitch	negligible
Photomultiplier	Hamamatsu R2487
Geometry	
Center-detector distance	variable
Axial FOV	40 mm diameter
Transaxial FOV	40 mm
Data	
Data acquisition	3D, List mode
Reconstruction	2D, ML-EM
Rebinning	Multiple slice rebinning
Performance	
Resolution	2.1 mm
Sensitivity	120cps/μCi (3.24cps/kBq) for 8 cm center-detector distance; no dynamic energy discrimination (see Section A)

III. FRONT-END ELECTRONICS

A standard resistive divider system is used for the readout of the crossed wire anode of the PMT. The four signals, two for the x- and two for the y-direction, are read out into four preamplifiers and shaping amplifiers. The output signals are normalized to the sum pulses ($x1 + x2$ and $y1 + y2$) and

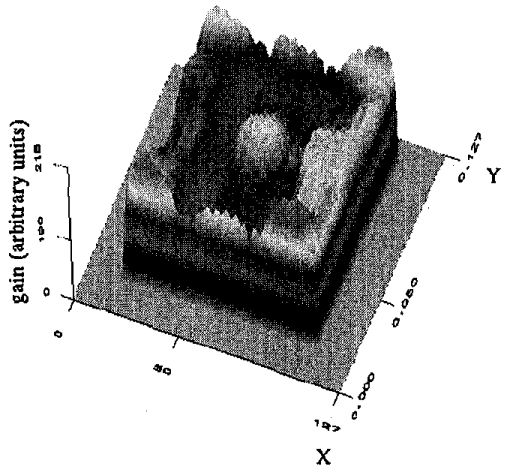

Figure 3: Position dependent gain inhomogeneity of a position sensitive photomultiplier tube

fed into two dividing 9Bit Flash-ADCs for determining the x and y addresses ($x = \frac{x1}{x1+x2}, y = \frac{y1}{y1+y2}$) and into a sum pulse ADC (x1+x2+y1+y2) for pulse height analysis. The resulting three 8Bit data words are transferred to an EISA PC-Board which acts as a Bus-Master-ADC-Controller (BMAC). This PC plugin board is based on a LCA-array XILINX-chip allowing programmable configurations with respect to various applications. During a measurement, the BMAC module checks the coincidence condition with a coincidence timing window of 250 ns and stores the ADC values for the position as well as for the energy in list mode.

Position sensitive PMT's have a large position dependent gain variance (figure 3) which leads to large variations in signal height. This prohibits the setting of a fixed hardware level for energy discrimination, and one has to accept pulses in a broad range since otherwise the sensitivity of the detector varies considerably across the photocathode [13]. The hardware discriminator (one for each detector) acts as a global threshold just to suppress noise, and its lower level is set to a minimum.

IV. DATA PREPROCESSING

A. *Dynamic discriminator levels*

The energy discrimination can be performed during either data acquisition or data preprocessing. First, the energy spectra are measured using a homogeneous activity distribution and list mode data acquisition. A listmode data set consists of ADC values for the x- and y-locations of the two coincident detector modules as well as ADC values for the energy information. The data are analyzed and sorted according to the energy ADC values for each x-y location. In a second step the photopeak for each spectrum has to be found. The ADC values for the photopeak positions and the upper and lower discriminator levels which are calculated from the photopeak position are stored in a look-up table.

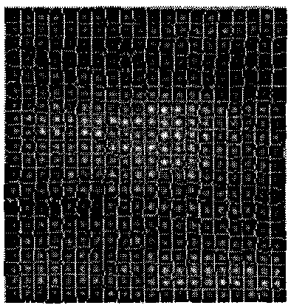

Figure 4: Crystal identification

B. Crystal identification and ADC-to-crystal conversion

The x-and y position ADC values have to be transformed into spatial coordinates. For this purpose, the four detectors are irradiated homogeneously, and the 2D images are recorded. The single crystals are clearly visible, which allows us to perform a segmentation of the crystal matrix by searching first the maximum in each single crystal and then looking for the gradients to decide which ADC values belong to the crystals. Figure 4 shows the segmentation of one detector.

Segmentation of each crystal array allows a lookup table to be constructed in which a range of ADC values are assigned to a particular crystal. The list mode data are transformed with this lookup table directly into crystal locations, a process that also corrects for spatial non-linearities in the detectors.

C. Rebinning and 2D sinograms

The 3D mode data are rebinned using a multiple slice rebinning method [14] which means that they are sorted (rebinned) into a stack of 2D sinograms with 180 angles and 128 projections. These data can then be reconstructed by applying the reconstruction algorithm to each slice separately. An oblique line of response (LOR) contributes to the sinograms of all slices which it transverses within the FOV. For the TierPET geometry, the maximum oblique angle and therefore the number of transversed slices is depending on the center-detector distance. With a center-detector distance of 10 cm, a diameter of the field of view of 4 cm and a slice thickness of 2 mm four slices can contribute to the LOR, with a center-detector distance of 24 cm only two slices are transversed. For this reason the axial filtering step which is described in [14] is neglected.

Since the estimation of attenuation correction factors based on transmission measurements is not yet possible, the factors are calculated assuming a homogeneous cylinder with $\mu = 0.095\text{cm}^{-1}$ during sinogram conversion. The points of intersection between the cylinder and the LOR are determined and the distance between these points is calculated. With this method only a rough estimation of attenuation correction factors can be obtained, and especially the attenuation caused by the object tablet or the fixation of the rat are neglected.

The images are reconstructed in 2D mode using a ML-EM algorithm [15]. Reconstruction time for one slice and 25 iterations is about 15 s on a DEC Alpha Station 200.

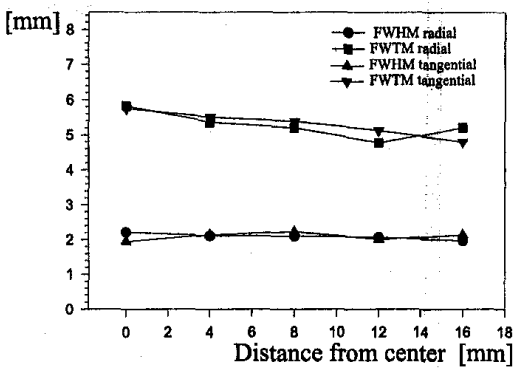

Figure 5: Spatial resolution of the TierPET, measured with a [^{18}F]-fluoride filled needle and reconstructed with 20 iterations. Center-detector distance: 12 cm.

The listmode data acquisition followed by conversion into sinograms allows us to change the detector distances between two time frames. The data acquisition starts with a count rate immediately below detector saturation, and the system sensitivity can be increased by reducing the detector distance when the count rate gets low due to physical decay or biological washout of the radiopharmaceutical.

V. TierPET Performance Evaluation

A. System Performance

The spatial resolution of the TierPET was measured using a [^{18}F]fluoride filled needle of 0.9 mm diameter placed in air. The full width at half maximum (FWHM) was obtained from line profiles using linear interpolation and correction for line source width by deconvolving the measured and line source profiles. The proposed spatial resolution of about 2 mm over the field of view could be confirmed by our measurements (figure 5).

The system sensitivity was measured with a low activity point source located in the center of the field-of-view using only the hardware discriminator. Figure 6 shows the sensitivity as a function of the center-detector distance. The maximum sensitivity amounts to 120 cps/μCi with a center-detector distance of 8 cm.

Both resolution and sensitivity data were taken without dynamic discriminator levels. The lower levels of the hardware discriminator amount to 180-280 keV depending on the position on the photocathode.

Scatter fraction was measured using a 6 cm diameter water filled phantom containing a line source at three different radial positions subsequently with a center-detector distance of 16 cm. The sinogram profiles were used to calculate the number of scattered events. For each projection angle and for 7 central slices, the pixel having the greatest value was found and the projection was shifted so that the pixel containing the maximum

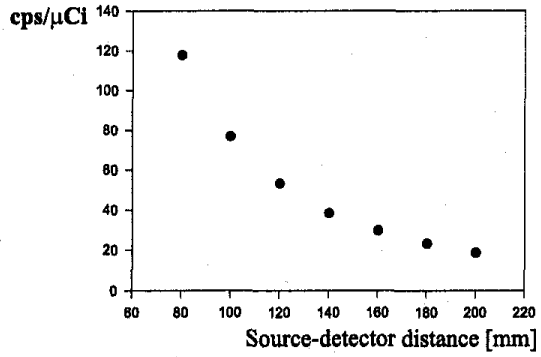

Figure 6: Sensitivity of the TierPET as a function of the center-detector distance.

value was aligned with the central pixel of the sinogram. For the determination of the scattered counts a polynomial function was fitted to the wings of the profile and extrapolated under the central peak. The total and scattered counts were weighted after decay correction by the area of the annulus at the respective radial position. The scatter fraction was calculated by taking the ratio of scattered and total counts. The measurement was performed for a dynamic discriminator level of 200 keV and 350 keV as well as without dynamic discrimination. The scatter fraction amounts to 15.3% (without discrimination), 12% (200 keV) and 10.1% (350 keV), respectively.

Noise equivalent count rate performance was measured using the same 6 cm diameter phantom with 110 ml ^{11}C ($t_{1/2}$=20.4 min) in solution, starting with an activity concentration of 48 μCi/ml. Center-detector distance was 16 cm. Random coincidences were measured using the delayed coincidence method. Total and random counts were collected in turn every 1.5 min without dynamic discrimination. Trues as well as noise equivalent counts (NEC) have been calculated following [16]. The trues and randoms count rate and the noise equivalent count rate performance is displayed in figure 7.

B. PHANTOM IMAGES

We have measured a small phantom representing the brain of a rat with cortex and striatum. All compartments of the phantom were filled with the same [^{18}F]fluoride activity concentration.

Figure 8 shows two slices of the reconstructed TierPET data. Below, the corresponding MR images delineate the shape of the phantom. The data were acquired with a center-detector distance of 150 mm and with angular steps of 7.5 °. During 120 minutes 4 million coincidence counts were acquired.

C. ANIMAL IMAGES

First animal studies were performed with the dopamine-D2 neuroreceptor ligand [^{18}F]methyl-benperidol [17], which exhibits a high uptake in the striatum. To demonstrate the potential of the TierPET for *in vivo* studies, a Sprague

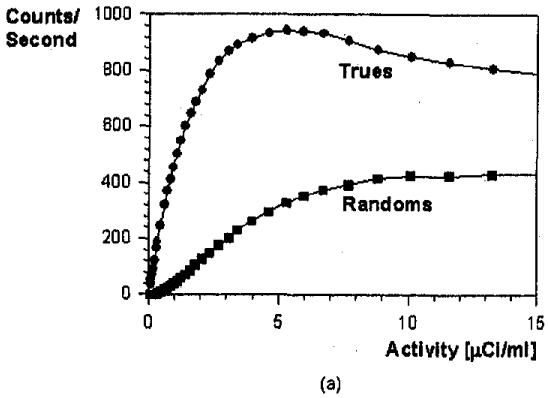

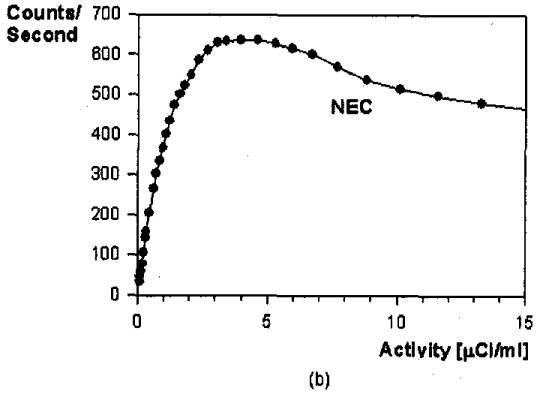

Figure 7: (a) Trues and random count rate performance; (b) Noise equivalent count rate performance.

Dawley rat was injected with 1.4 mCi (51.8MBq) [^{18}F]methyl-benperidol. Scanning was started 10 minutes after injection for 110 minutes. Center-detector distance was 130 mm. In total 3 million counts were recorded.

Figure 9 shows the reconstructed PET data together with a MRI scan of the rat. In addition to the striatum, the receptor ligand is taken up in two areas close to the eyes and an area near to the tongue. The distances between the two parts of the striatum as well as between the striatum and the areas close to the eyes are about 8 mm. These structures can be clearly separated because of the eight-fold improvement in volume resolution of the TierPET over clinical systems.

Figure 10 shows TierPET images of the [^{18}F]methyl-benperidol uptake in a dissected brain. For this experiment 1.8 mCi (66.6MBq) were injected into the rat. The rat was scanned from 10 minutes after injection to 55 minutes with center-detector distances of 160 mm and 120 mm. The brain of the rat was dissected 70 minutes after injection. The dissected brain was scanned for another 60 minutes. Center-detector distance was 80 mm, total quantity of counts > 1.1 million. The count rate of this scan was <100 cps compared to >1000 cps recorded just before dissection in the living rat applying the same center-detector distance. This means that the contribution of the brain to the data is below 10%. The strong accumulation of activity outside the brain leads to a distortion of the signals

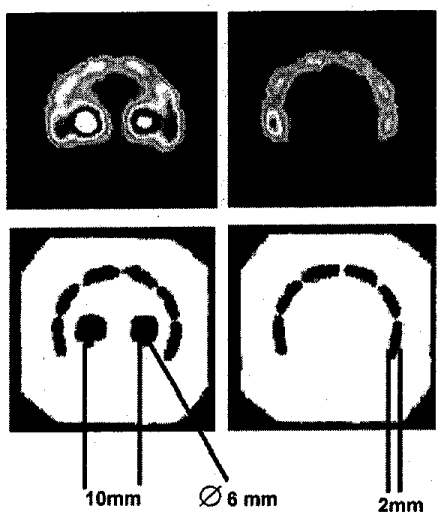

Figure 8: Phantom representing the brain of a rat (top: TierPET, bottom: MRI). All compartments were filled with the same [^{18}F]-fluoride activity concentration.

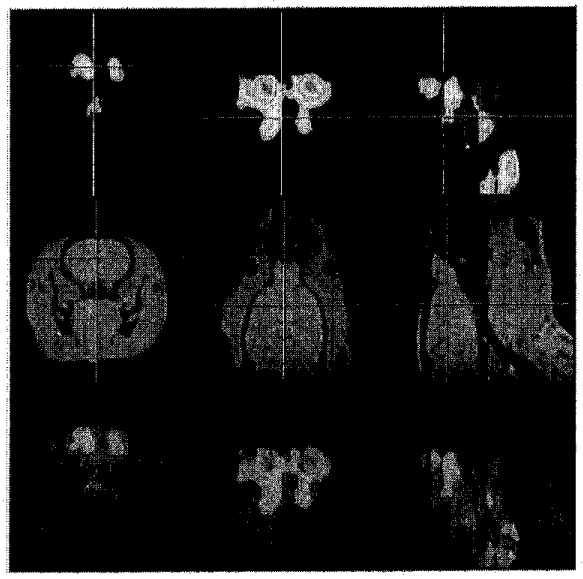

Figure 9: Rat brain: Uptake of the dopamine D2 receptor ligand [^{18}F]methyl-benperidol in the rat. Injected activity: 1.4 mCi. Sum image from 10-120 minutes after injection. From left to right: Coronal view, transversal view, sagittal view. From top to bottom: TierPET data, MRI data, Superposition of TierPET and MRI data.

deriving from the brain. In order to correct for this impairment appropriate corrections have to be developed.

VI. PERSPECTIVES AND DISCUSSION

The initial results obtained from the TierPET are encouraging and agree with earlier simulation results. The proposed resolution of about 2 mm in all dimensions has been achieved. Due to the low Z of YAP the sensitivity of the scanner is limited. As a consequence, the imaging time amounts to about 1 hour for the scans reported here. This may be a limitation when imaging the uptake of short half-life radiopharmaceuticals. Dynamic imaging is feasible by taking data in sections of, for example, 10 scans, each with 6 minutes imaging time. The low sensitivity of the scanner may be improved by using LSO.

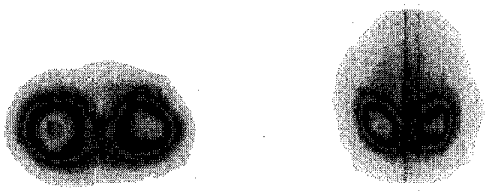

(a) Coronal view (b) Transversal view

Figure 10: Rat brain: Uptake of the dopamine D2 receptor ligand [^{18}F]methyl-benperidol in the caudate putamen of a rat brain. Injected activity: 1.8 mCi. Brain dissected 70 minutes after injection. Sum image from 90-150 minutes after injection.

A new kind of front-end electronics could improve the randoms fraction by shortening the coincidence timing window. Due to the small volumes which are scanned by the TierPET, the width of the coincidence timing window is not really a limiting factor, even though it is still worth to be improved.

The activity quantification can be achieved by applying corrections both for the scattered and the attenuation compensation to the recorded emission data. In order to estimate the scattered fraction, the rate of scattered photons taking part in a measured projection, an analytic method using the Klein-Nishina equation will be included in the reconstruction program. Together with the absorbed photons the non-detected scattered photons contribute to the attenuation fraction. On account of the errors associated with the calculated attenuation correction, a system of attenuation correction based on transmission measurements [18] is under development: two collimated point positron-sources are employed, non-simultaneously with emission measurements, to obtain the blank (without object) and transmission (with object) scans. The reconstructed attenuation image will be segmented in order to reduce statistical variations. The correction factors, derived by reprojecting, are then applied to the emission projections.

The image quality of the scanner may be further improved by using a 3D reconstruction [19], [20], [21]. We are currently working on an iterative 3D reconstruction program testing various reconstruction algorithms [22],[23], [24]. The precise calculation of the projection matrix as well as the 3D reconstruction will be parallelized. The reconstruction volume will be based on polar coordinates. This increases symmetries in the calculation of the projection matrix and allows a reduction of memory required for the storage of the matrix.

VII. ACKNOWLEDGMENTS

This work contains in part the contents of the Ph.D. thesis of Andreas Terstegge.

The animal studies were performed in preparation of a cooperative study with the Nuklearmedizinische Klinik, Heinrich-Heine-Universitaet Duesseldorf, to evaluate the TierPET.

The MRI scan of the rat was performed by Dr. J. Shah, Institute for Medicine, Forschungszentrum Juelich GmbH. The TierPET and MRI data (figure 9) are displayed using the MPI tool developed by the Max-Planck-Institute for Neurological Research, Cologne, Germany.

VIII. REFERENCES

[1] P. M. Bloomfield, R. Myers, S. P. Hume, T. J. Spinks, A. A. Lammertsma, and T. Jones, "Three dimensional performance of a small-diameter positron emission tomograph," *Phys. Med. Biol.*, vol. 42, p. 389, 1997.

[2] P. Bruyndonckx, X. Liu, S. Tavernier, and S. Zhang, "Performance study of a 3D small animal PET scanner based on BaF_2 crystals and a photo sensitive wire chamber," *Nucl. Instrum. and Meth. A*, vol. 392, p. 407, 1997.

[3] S. R. Cherry, Y. Shao, R. W. Silverman, K. Meadors, S. Siegel, A. Chatziioannou, J. W. Young, W. F. Jones, J. C. Moyers, D. Newport, A. Boutefnouchet, T. H. Farquhar, M. Andreaco, M. J. Paulus, D. M. Binkley, R. Nutt, and M. E. Phelps, "MicroPET: A high resolution PET scanner for imaging small animals," *IEEE Trans. Nucl. Sci.*, vol. 44, no. 3, p. 1161, 1997.

[4] R. Lecomte, J. Cadorette, S. Rodrigue, D. Lapointe, D. Rouleau, M. Bentourkia, R. Yao, and P. Msaki, "Initial results from the Sherbrooke avalanche photodiode positron tomograph," *IEEE Trans. Nucl. Sci.*, vol. 43, no. 3, p. 1952, 1996.

[5] M. Watanabe, H. Okada, K. Shimizu, T. Omura, E. Yoshikawa, T. Kosugi, S. Mori, and T. Yamashita, "A high resolution animal PET scanner using compact PS-PMT detectors," *IEEE Trans. Nucl. Sci.*, vol. 44, no. 3, p. 1277, 1997.

[6] W. W. Moses, P. R. G. Virador, S. E. Derenzo, R. H. Huesman, and T. F. Budinger, "Design of a high-resolution, high-sensitivity PET camera for human brains and small animals," *IEEE Trans. Nucl. Sci.*, vol. 44, no. 4, p. 1487, 1997.

[7] J. L. Robar, C. J. Thompson, K. Murthy, R. Clancy, and A. M. Bergman, "Construction and calibration of detectors for high-resolution metabolic breast cancer imaging," *Nucl. Instrum. and Meth. A*, vol. 392, no. 1-3, p. 402, 1997.

[8] A. del Guerra, F. de Notaristefani, G. di Domenico, M. Giganti, R. Pani, A. Piffanelli, A. Turra, and G. Zavattini, "Use of a YAP:Ce matrix coupled to a position-sensitive photomultiplier for high resolution positron emission tomography," *IEEE Trans. Nucl. Sci.*, vol. 43, no. 3, p. 1958, 1996.

[9] O. Fries, S. M. Bradbury, J. Gebauer, I. Holl, E. Lorenz, D. Renker, and S. Ziegler, "A small animal PET prototype based on LSO crystals read out by avalanche photodiodes," *Nucl. Instrum. and Meth. A*, vol. 387, p. 220, 1997.

[10] Preciosa Crytur, CZ - 51119 Turnov. Czech Republic.

[11] S. Weber, A. Terstegge, H. Herzog, R. Reinartz, P. Reinhart, F. Rongen, H. W. Mueller-Gaertner, and H. Halling, "The design of an animal PET: Flexible geometry for achieving optimal spatial resolution or high sensitivity," *IEEE Trans. Med. Imaging*, vol. 16, no. 5, p. 684, 1997.

[12] S. Weber, A. Terstegge, R. Engels, H. Herzog, R. Reinartz, P. Reinhart, F. Rongen, H. W. Mueller-Gaertner, and H. Halling, "The KFA TierPET: Performance characteristics and measurements," in *Nuclear Science Symposium & Medical Imaging Conference, IEEE Conference Record*, p. 1117, 1996.

[13] M. Kanyo, R. Reinartz, J. Schelten, and K. D. Mueller, "Two-dimensional neutron scintillation detector with optimal gamma discrimination," *Nucl. Instrum. and Meth. A*, vol. A320, p. 562, 1992.

[14] R. M. Lewitt, G. Muehllehner, and J. Karp, "Three-dimensional image reconstruction for pet by multi-slice rebinning and axial image filtering," *Phys. Med. Biol.*, vol. 39, pp. 321–339, 1994.

[15] B. Lipinski, H. Herzog, E. Rota Kops, W. Oberschelp, and H. Mueller-Gaertner, "Expectation maximization reconstruction of positron emission tomography images using anatomical magnetic resonance information," *IEEE Trans. Med. Imaging*, vol. 16, no. 2, p. 129, 1997.

[16] S. C. Strother, M. E. Casey, and E. J. Hoffman, "Measuring PET scanner sensitivity: relating countrates to image signal-to-noise ratios using noise equivalent counts," *IEEE Trans. Nucl. Sci.*, vol. 37, no. 2, p. 783, 1990.

[17] K. Hamacher and W. Hamkens, "Remote controlled one-step production of ^{18}F labeled butyrophenone neuroleptics exemplified by the synthesis of n.c.a. [^{18}F] N-methylspiperone," *Appl. Radiat. Isot.*, vol. 46, no. 9, p. 911, 1995.

[18] P. A. McNeil, P. J. Julyan, and D. J. Parker, "An attenuation measurement technique for rotating planar detector positron tomographs," *Phys. Med. Biol.*, vol. 42, p. 1633, 1997.

[19] J.-S. Liow, S. C. Strother, K. Rehm, and D. A. Rottenberg, "Improved resolution for PET volume imaging through three-dimensional iterative reconstruction," *J. Nucl. Med.*, vol. 38, pp. 1623–1631, 1997.

[20] C. A. Johnson, J. Seidel, R. E. Carson, W. R. Gandler, A. Sofer, M. V. Green, and M. E. Daube-Witherspoon, "Evaluation of 3D reconstruction algorithms for a small animal PET camera," *IEEE Trans. Nucl. Sci.*, vol. 44, no. 3, pp. 1303–1308, 1997.

[21] J. Qi, R. M. Leahy, S. R. Cherry, A. Chatziioannou, and T. H. Farquhar, "High-resolution 3D bayesian image reconstruction using the microPET small animal scanner,"

Phys. Med. Biol., vol. 43, pp. 1001–1013, 1998.

[22] G. H. Golub and C. F. Van Loan, "Matrix computations," in *Johns Hopkins Series in the Mathematical Sciences*, Johns Hopkins University Press, Dec. 1996.

[23] L. A. Shepp and Y. Vardi, "Maximum likelihood reconstruction for emission tomography," *IEEE Trans. Med. Imaging*, vol. MI-1, pp. 113–122, Oct. 1982.

[24] R. Gordon, R. Bender, and G. T. Herman, "Algebraic reconstruction techniques (ART) for three-dimensional electron microscopy and x-ray photograpy," *Journal of Theoretical Biology*, vol. 29, pp. 471–481, 1970.